POLITECNICO DI TORINO
Repository ISTITUZIONALE

ACTIVE FLOW CONTROL OF AN OVER-EXPANDED NOZZLE BY SHOCK VECTOR CONTROL

(Article begins on next page)

30 June 2024

ACTIVE FLOW CONTROL OF AN OVER-EXPANDED NOZZLE BY SHOCK VECTOR CONTROL

Simone Rizzo[1], Michele Ferlauto[2] and Roberto Marsilio[3]

[1] Politecnico di Torino, c.so Duca degli Abruzzi 24, 10129 Turin, Italy,
simone.rizzo@studenti.polito.it

[2] Politecnico di Torino, c.so Duca degli Abruzzi 24, 10129 Turin, Italy,
michele.ferlauto@polito.it   http://staff.polito.it/michele.ferlauto

[3] Politecnico di Torino, c.so Duca degli Abruzzi 24, 10129 Turin, Italy,
roberto.marsilio@polito.it

Key words: Nozzle flow, Flow Control, Fluidic Thrust-Vectoring

Abstract.   *Thrust vectoring obtained by the nozzle flow manipulation technique known as Shock Vector Control (SVC) is investigated numerically. In the shock vector control method, a shock structure is generated in the main flow by using transversal continuous blowing. The pressure distribution on the nozzle walls becomes asymmetric, thus giving rise to a lateral force. The open-loop response of the nozzle and the thrust vectoring effectiveness/controllability are investigated by using a CFD tool based on the compressible URANS equations. Nozzle performances and thrust vector angles have been computed for different nozzle pressure ratios in the range of over-expanded conditions. The latter represent the worst case, where the shock structure generated by the control is amplified by the re-compression requirements imposed by the external ambient pressure.*

1   INTRODUCTION

Active flow control in supersonic nozzle mainly concerns strategies for Fluidic Thrust Vectoring (FTV) [1–3]. Actual thrust vectoring technology is based on movable nozzles but the jet-vectoring effect of nozzle deflection can be also generated by active flow control devices on fixed nozzles. For this reason, approaches based on active flow control are under investigation. Thrust vectoring offers many advantages in terms of safety, maneuverability and effectiveness of aircraft controls, by helping the vehicle to meet take-off and landing requirements and by enhancing the controls at low dynamic pressures, where aerodynamic devices are less effective [4]. These considerations have pushed the research towards innovative approaches to thrust vectoring. Fluidic thrust-vectoring retains the advantages of mechanical thrust vectoring without the need of the complex adjustable hardware of the variable geometry devices [3]. FTV in fixed symmetric nozzles is obtained, for instance, by a local blowing at wall that causes flow separations and asymmetric pressure distributions, thus allowing the vectoring of primary jet thrust. The FTV technology

does not increase significantly the aircraft weight and can be applied to systems that were not originally designed with such feature. The key point for the fluidic approach is anyway the identification of a manipulation technique that can modulate gradually the symmetry-breaking effect within an acceptable range of deterioration of the nozzle performances [4].

Several manipulation strategies have been investigated in the literature for such purpose. FTV approaches include the Shock Vector Control (SVC) [5,6], counter-flow methods [7–10], the throat shifting and the supersonic dual-throat nozzle [1, 11–13]. The performances of these approaches have been measured in terms of control efficiency and thrust loss. The efficiency of vectoring is computed as the degree of vectoring achieved per percent of secondary flow required as compared to the primary nozzle flow. All these methods require continuous blowing of secondary flow or other kind of air-spillage or bleed, but the counter-flow method. In fact, the latter requires additional equipments in order to provide the suction between the trailing edge of the nozzle and the aft-collar [1].

Since jet-vectoring results from the breaking of wall pressure symmetry, flow manipulation approaches other than continuous blowing can be followed. For instance, one can induce forcing by means of synthetic jets [14, 15] or plasma actuators [16]. In order to explore the feasibility of such approaches, numerical tools are the privileged means of investigation for evaluating the steady and unsteady nozzle performances [4, 9] Unsteady CFD analyses can help in deriving the time-varying nozzle performances, in clarifying the role and interaction between various nonlinear phenomena, in assessing and testing the open/closed-loop control laws [11, 12].

In present work we focused on the controllability of a fixed nozzle, with a special attention to application for hypersonic vehicle and space launchers. It such case, is well-known that at ground level the nozzle is strongly over-expanded by design and therefore a complex shock structure appears in order to match the flowfield with the ambient discharge pressure. A promising candidate for the FTV of these nozzles is the shock vector control. The application of the shock vector control is investigated here numerically with the aim of testing the control effectiveness of the rocket nozzle and the system sensitivity to different forcing actions. URANS analyses are used for computing the unsteady nozzle performances [12], with the aim of investigating the nonlinear dynamics of the shock structures under forcing and their controllability. Where available, the numerical results are compared with experimental data found in the open literature [2, 17].

2   NOZZLE SETUP

The nozzle geometry under investigation is based on the configuration studied at Nasa LARC. The reader is referred to Ref. [2] for the details on the setup and testing conditions. In present configuration the nozzle is endowed with two blowing slots, in the upper *(up)* and in the lower *(lw)* wall, as shown in Figure 1a. This allows for the thrust vectoring modulation upwards and downwards. In order to represent the system forcing by a single input that manages both blowing slots, the two signals are combined in a single input as expressed in Ref. [12]. It is also assumed that just one actuator at time is active. The resulting open-loop control logic of the nozzle system is represented in Figure 1b.

(a)
(b)
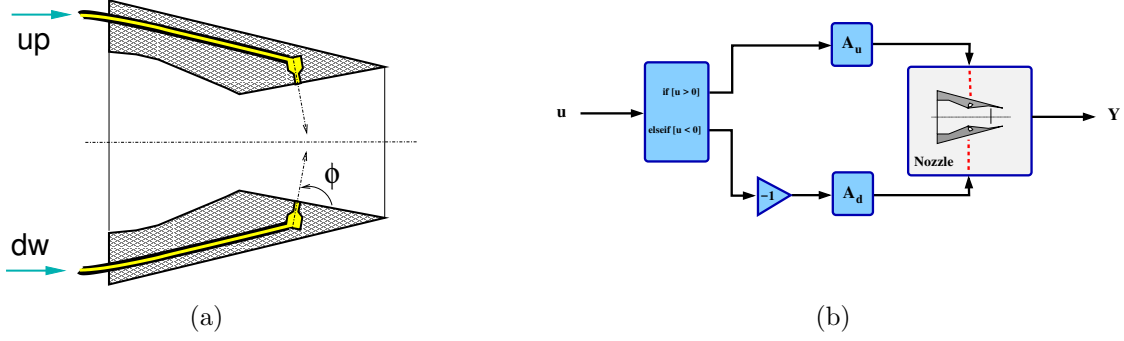
Figure 1: Sketch of (a) the secondary jet actuation system and (b) the open-loop scheme of nozzle control.

MATHEMATICAL MODEL

The flow governing equations are the compressible Unsteady Reynolds Averaged Navier-Stokes equations (URANS) written in the compact integral form

$$\frac{\partial}{\partial t} \int_v \vec{W} \, d\mathcal{V} + \int_\mathcal{S} \vec{F}_I \cdot \hat{n} d\mathcal{S} + \int_\mathcal{S} \vec{F}_V \cdot \hat{n} d\mathcal{S} = \int_\mathcal{V} \vec{H} d\mathcal{V} \tag{1}$$

in an arbitrary volume $\mathcal{V}$ enclosed in a surface $\mathcal{S}$. With usual conventions, $\vec{W} = \{\rho, \rho\vec{q}, E, \tilde{\nu}_t\}^T$ is the hyper-vector of conservative variables, $\vec{F}_I$ and $\vec{F}_V$ are tensors containing the inviscid and the viscous fluxes, respectively.

$$\vec{F}_I = \left\{ \rho\vec{q}, p\bar{\bar{I}} + \rho\vec{q} \otimes \vec{q}, (E+p)\vec{q}, \tilde{\nu}_t\vec{q} \right\}^T, \tag{2}$$

$$\vec{F}_V = \frac{\sqrt{\gamma M_\infty}}{\text{Re}_\infty} \left\{ 0, -\bar{\bar{\tau}}, -\kappa\nabla T - \bar{\bar{\tau}} \cdot \vec{q}, -\frac{\nu + \tilde{\nu}_t}{\sigma}\nabla\tilde{\nu}_t \right\}^T \tag{3}$$

$\vec{q} = \{u, v, w\}^T$ is the velocity vector, E the total energy per unit volume, M_∞ and Re_∞ are the free-stream Mach number and the Reynolds number, γ is the ratio of the specific heats and $\bar{\bar{I}}$ is the unit matrix. The term $\vec{H}$

$$\vec{H} = \left\{ 0, 0, 0, c_{b1}\tilde{S}\tilde{\nu}_t + \frac{c_{b2}}{\sigma}\left(\nabla\tilde{\nu}_t\right)^2 - c_{w1}f_w\left(\frac{\tilde{\nu}_t}{d}\right)^2 \right\}^T \tag{4}$$

contains turbulence model source terms. System (1) is reduced to non-dimensional form with respect to the following reference values: L for length, ρ_∞ for density, T_∞ for temperature, $\sqrt{RT_\infty}$ for velocity, RT_∞ for energy per unit mass and μ_∞ for viscosity. The viscous stresses are $\tau_{ij} = (\mu + \mu_t)\left[\frac{\partial q_j}{\partial x_i} + \frac{\partial q_i}{\partial x_j} - \frac{2}{3}\left(\nabla \cdot \vec{q}\right)\delta_{ij}\right]$. The laminar viscosity μ is computed via the Sutherland's law, whereas the turbulent viscosity $\mu_t = \rho\nu_t$ is defined according to the Spalart-Allmaras (S-A) model. [18, 19] Despite its simplicity, the S-A model has shown a closer agreement with the experimental data for the case of unsteady

3
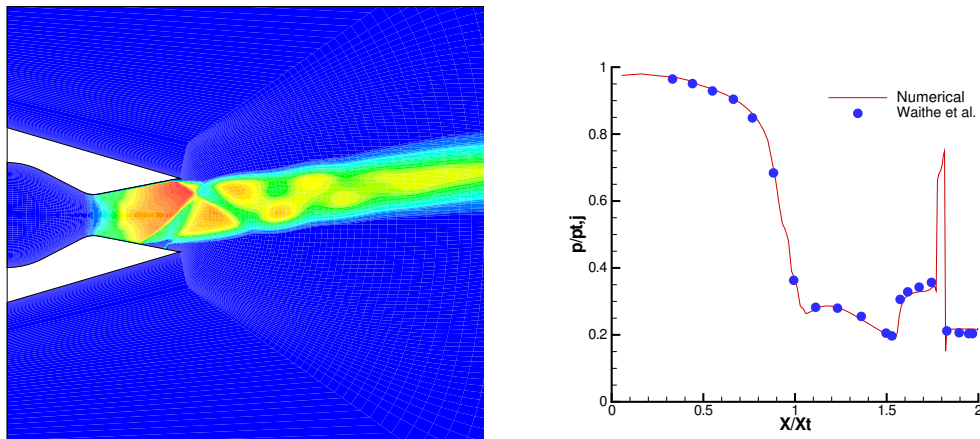
Figure 2: Comparison of numerical and experimental results.

or pulsatile flow, when compared to $k - \epsilon$ and $k - \omega$ SST models [20–22]. The numerical solution of system (1) is based on a Godunov method with Flux-Difference Splitting (FDS) and an Essentially Non-Oscillatory (ENO) scheme [23] second order accurate in both time and space. The integration in time is carried out according to a 4th order Runge Kutta scheme. Further numerical details, as well as the code validation for the case of thrust vectoring can be found in Refs. [11, 12]. The numerical method has been efficiently parallelized by using OpenMP directives. The spatial and time accuracy of the solver has been widely tested in many unsteady flowfields as, for instance, the flow manipulation by synthetic jets and the post-stall control of NACA0015 profile [20]; the simulation of rotating stall generation and evolution; time-dependent flows with moving grids and inverse problems [24]; the computation of aeroelastic standard configurations and blade flutter.

3 NUMERICAL RESULTS

3.1 Nasa LARC Nozzle Test-case

Numerical and experimental testing of a supersonic nozzle for SVC thrust-vectoring have been carried out at Nasa Langley Research Center (LARC) [2]. The FTV performances of a 2D nozzle were evaluated for different levels of the nozzle pressure ratio and injection pressure. The latter is defined in [2] by means of the Secondary Pressure Ratio (SPR), i.e. the ratio between the total pressure of the secondary jet and the total pressure of the main (or primary) jet flow. Different position of the injection point and different widths of the blowing slot were also considered. Experimental studies on the primary jet behavior with and without flow manipulation at different levels of NPRs are reported [2]. The above-mentioned investigation represents a reference test-case for our study on the
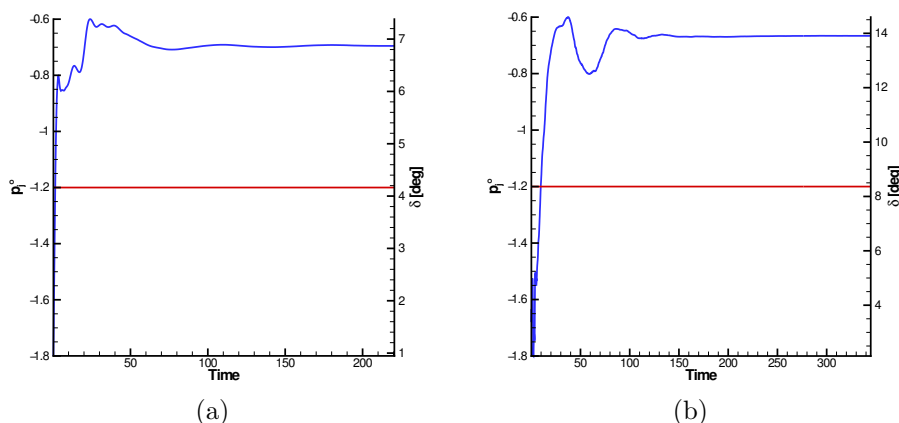
Figure 3: Step response of the nozzle system at (a) NPR = 4.6 and (b) NPR = 2 .

active control of supersonic nozzles by means of SVC strategies.

A one-dimensional approximation of the Nasa LARC nozzle let us estimate an adaptation pressure ratio NPR $\simeq$ 8.8. The investigations carried out in Ref. [2] covers the range $2 <$ NPR < 10. A typical nozzle pressure ratio of the tests is NPR=4.6, i.e. a value that corresponds to a condition of moderate over-expansion.

We start the analysis by the numerical simulation of the nozzle flow under SVC forcing at NPR = 4.6 . The secondary slot at the nozzle lower wall is activated according to the blowing condition of the experimental tests [2]. The computed flowfield in terms of Mach number iso-lines is presented in Figure 2a, where the shock structure, the separation zones and the secondary jet are clearly visible. Since the lower slot has been activated, the flow is deflected upwards. Let us also note that, although being the NPR about the half of that of the theoretical adaptation, the flow at the unmanipulated (upper) wall is still fully attached. For this reason, the nozzle can be considered as moderately over-expanded. The computed and the experimental pressure distributions along the lower wall of the nozzle are compared in Figure 2b. The results show a very good agreement.

3.2   Open-Loop Dynamics

The open-loop dynamics of the system is then investigated numerically in the same spirit of Refs. [11,12] by applying classical forcing functions. For instance, step forcing is a typical approach adopted in automatic controls theory in order to disclose the characteristics of a dynamical system. The dynamic responses of the nozzle to secondary blowing following a step in time are presented in Figure 3 for the case at NPR = 2 and NPR = 4.6, respectively. A remarkable difference of the system transient can be appreciated, although the starting point is the symmetric jet configuration in both cases. This difference let us suppose that the stability characteristics at the selected NPR's are different, as further tests will show. Moreover, at NPR = 2 the nozzle flow is strongly over-expanded and characterized by a shock structure in the middle of the diverging portion of the nozzle, with large flow separations. This condition make the system very sensitive to shock-boundary layer interactions.

5
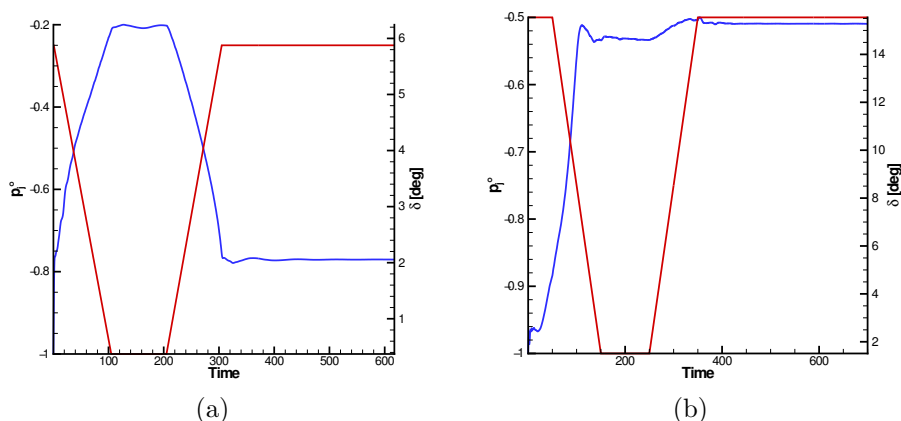
Figure 4: Open-loop response of the nozze system at (a) NPR = 4.6 and (b) NPR = 2 . Negative pressure levels refer to the lower slot and must be read in absolute value, according to Ref. [12].

A more realistic forcing is obtained by imposing a ramp, instead of a step, as forcing law. Starting from the unmanipulated case corresponding to the symmetric jet flow condition, blowing is activated at lower wall and the intensity is increased in time until a prescribed maximum value is reached. The blowing intensity is maintained constant for a while, thus allowing the system to reach a steady state, and then the forcing action is decreased linearly in time by following a second ramp law. At the prescribed minimum constant forcing the system is let to assess to the new steady state. The forcing function imposed as well as the system responses are shown in Figure 4. At NPR = 4.6, the system response follows the forcing action with a minimal time lag and overshoot during both the increasing and decreasing ramps (see Figure 4a). Moreover, the system tends to recover the symmetric condition when forcing is ceased. Some snapshots of the flowfield during the transient evolution are presented in Figure 5.

When the same forcing is applied to the nozzle system at NPR = 2, a quite different flow evolution is obtained, thought the initial condition is symmetric as in previous case. The system response is shown in Figure 4b. As visible, the thrust angle increases as the secondary flow injection increases, but the system does not relax again to the symmetric solution after forcing is ceased: it assess itself to a new, unsymmetrical, steady state. A detailed analysis of the open-loop dynamics as well as of the flow evolution during the transients at low nozzle pressure ratios is carried out in Ref. [25] and it is not reported here for conciseness.

The existence of the unsymmetrical steady/unsteady flow configurations in supersonic nozzles with low divergence angles has experimental evidences [26, 27] and it is caused by the complex and nonlinear interaction between boundary layer separation and shock patterns. The higher the over-expansion condition of the nozzle is, the closer the shock structures to the throat are, the larger the separation zone that follow.

At strong over-expansion conditions, the nozzle system remains controllable by SVC but simple open-loop control laws are not effective anymore, because the system moves towards different equilibrium configurations at different NPRs. This can be explained by observing that the nozzle system has more than one equilibrium configuration and the
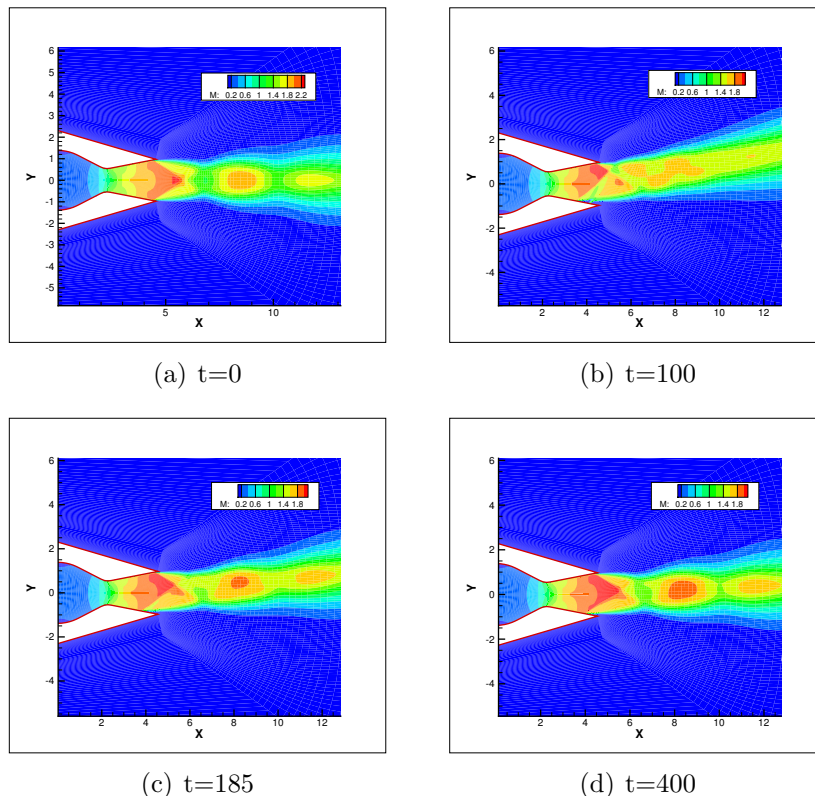
Figure 5: Snapshots of the Mach number flowfield during SVC forcing at NPR = 4.6 .

stability of these configurations changes at different NPRs. In this case, closed-loop control strategies are better suited.

3.3   Stability of the Symmetric Flow Solution

An approximation of the critical NPR-value is now sought, in order to identify the range of stability of the symmetric equilibrium solution. The approach adopted here in identifying the limit condition is somehow inspired to that used by Ziegler & Nichols in the ultimate cycle method [28]. A key-parameter, e.g. the NPR in our case, is modified and the system dynamics is investigated until a pure sinusoidal evolution is observed. In terms of linear stability, this condition corresponds to the dynamics of a linear system $\{\dot{X}\} = [A]\{X\}$ when the eigenvalues λ_i of the matrix $[A]$ are purely imaginary, that is when $\Re(\lambda_i) = 0$.

In present procedure, the nozzle flow is started from an fully unsymmetric, unsteady flow solution with $\delta \simeq 7^o$. The selected value of NPR is imposed and the free dynamics of the nozzle flow is computed. No blowing is applied. For certain NPR-values, the system is observed to converge to the symmetric solution and thus is $\delta = 0$, finally. For instance, at a nozzle pressure ratio as low as NPR = 2.8 the system converges to the symmetric solution after a series of damped oscillations. The computed dynamics is shown is Figure 6a.

The convergence rate of the system to the symmetric solution becomes weaker and

7
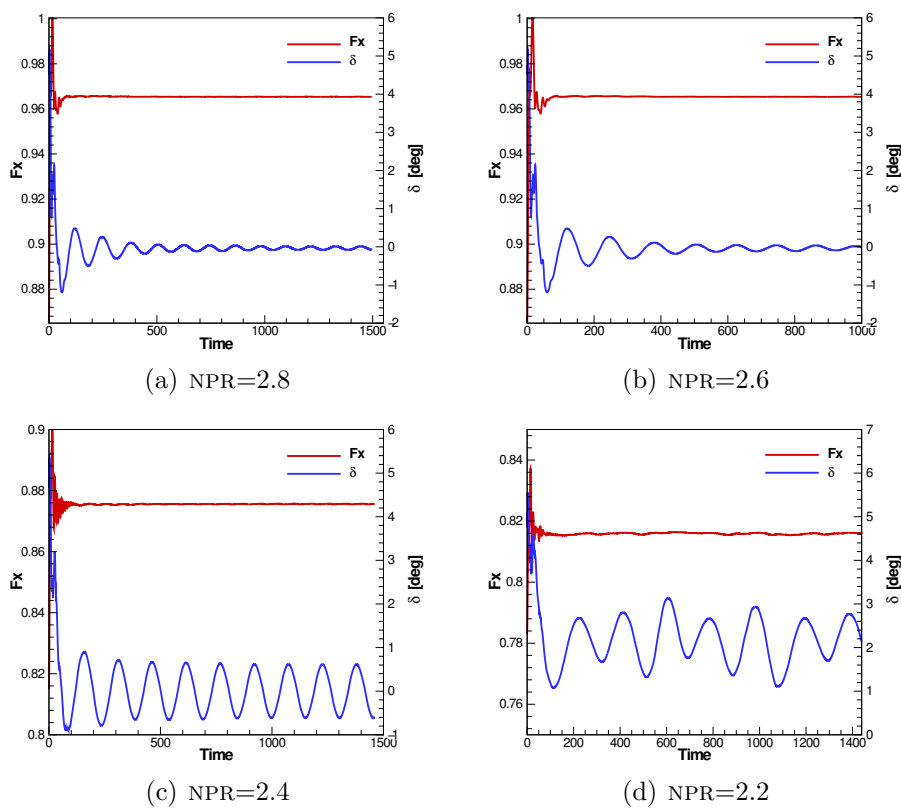
Figure 6: Free evolution in time of the system starting from the same configuration with $\delta \simeq 7^o$. Time history of the axial force F_x and thrust angle δ at different nozzle pressure ratios.

weaker, as far as the over-expansion degree is increased. At NPR $= 2.6$ the system still converges to $\delta = 0$ but the oscillations amplitude increases, as visible in Figure 6b . When a NPR $\simeq 2.4$ is prescribed, the system exhibits a dynamic response characterized by the series of sinusoidal, nearly undamped oscillations shown in Figure 6c . At lower NPRs the oscillations are amplified in time and also the mean value of the thrust angle $\delta \neq 0$ as visible in Figure 6d.

4   CONCLUSIONS

A computational tool assessed for the simulation of actively controlled flow and FTV in nozzles has been presented. The FTV applies strategies of active flow control on fixed nozzle in order to realize jet-vectoring effects otherwise obtained by deflecting a movable nozzle. The numerical method was validated previously for test-cases of other FTV manipulation techniques [1,11,17]. In present work the numerical tool is extended in order to include the simulation of nozzle flow forcing by the shock vector control method. The numerical procedure has been checked against an SVC test-case available in the open literature [2]. The paper also focused on the complex interactions that take place when the nozzle is operating at middle and strong over-expanded conditions. Control effectiveness in managing the FTV at different pressure ratios is investigated and the feasibility of

control is discussed.

5 ACKNOWLEDGMENTS

REFERENCES

[1] K.A. Deere. Summary of fluidic thrust vectoring research conducted at Nasa Langley Research Center. *21st AIAA Appl. Aerodyn. Conf., AIAA-2003-3800*, 2003.

[2] K.A. Waithe and K.A. Deere. An experimental and computational investigation of multiple injection ports in a convergent-divergent nozzle for fluidic thrust vectoring. *21st AIAA Applied Aerodynamics Conference, AIAA paper 2003-3802*, 2003.

[3] P.J. Yagle, D.N. Miller, K.B. Ginn, and J.W. Hamstra. Demonstration of fluidic throat skewing for thrust vectoring in structurally fixed nozzles. *ASME J. of Eng. for Gas Turb. and Pow.*, (2001), **123(3)**:502–507.

[4] K.A. Deere, J.D. Flamm, B.L. Berrier, and S.K. Johnson. Computational study of an axisymmetric dual throat fluidic thrust vectoring nozzle for a supersonic aircraft application. *43rd AIAA Joint Prop. Conf., AIAA 2007-5085*, 2007.

[5] M.R. Schaefermeyer. Aerodynamic thrust vectoring for attitude control of a vertically thrusting jet engine. *MSc in mechanical Engineering, Utah State University*, 2002.

[6] P.I.A. Wilde, W.J. Crowther, A. Buonanno, and A. Savvaris. Aircraft control using fluidic maneuver effectors. *26th AIAA Applied Aerodynamics Conference, AIAA paper 2008-6406*, 2008.

[7] P.J. Strykowski, A. Krothapalli, and D.J. Forliti. Counterflow thrust vectoring of supersonic jets. *AIAA Journal*, (1996),**34**:2306–2314.

[8] J.Y. Heo and H.G. Sung. Fluidic thrust-vector control of supersonic jet using coflow injection. *Journal of Propulsion and Power*, (2012), **28(4)**:858–861.

[9] R.Y. Deng and H.D. Kim. A CFD study on the counterflow thrust vector control. *Journal of Korean Society of Propulsion Engineers*, (2015), **44**:125–130.

[10] M.R. Van der Veer and P.J. Strykowski. Counterflow thrust vector control of subsonic jets: continuous and bistable regimes. *Journal of Propulsion and Power*, (1997), **13(3)**:412–420.

[11] M. Ferlauto and R. Marsilio. A numerical method for the study of fluidic thrust vectoring. *Advances in Aircraft and Spacecraft Science*, (2016), **3(4)**:367–378.

[12] M. Ferlauto and R. Marsilio. Numerical investigation of the dynamic characteristics of a dual-throat nozzle for fluidic thrust-vectoring. *AIAA Journal*, (2017), **55(1)**:86–98.

[13] C.S. Shin, H.D. Kim, T Setoguchi, and S. Matsuo. A computational study of thrust vectoring control using dual throat nozzle. *Journal of Thermal Science*, (2010), **19(6)**:486–490.

[14] D. Guo, A.W. Cary, and R.K. Agarwal. Numerical simulation of vectoring of a primary jet with a synthetic jet. *AIAA Journal*, (2003), **41(12)**:486–490.

[15] M. Ferlauto and R. Marsilio. On the use of synthetic jet actuators to induce jet-vectoring in nozzles. *Paper AIAA 2018-1627, AIAA Aerospace Sciences Meeting, Kissimmee, Florida*, 2018.

[16] D.R. Gonzalez, D.V. Gaitonde, and M.J. Lewis. Large-eddy simulations of plasma-based asymmetric control of supersonic round jets. *Int. Journal of Computational Fluid Dynamics*, (2015), **29(3–5)**:240–256.

[17] C.A. Bright, S.L. Tuttle, and A.J. Needly. The effect of vacuum on shock vector control performance. *19th Australian Fluid Mechanics Conference, Melbourne, Australia*, 2014.

[18] P.R. Spalart and S.R. Allmaras. A one-equation turbulence model for aerodynamic flows. *La Recherche Aerospatiale*, (1994), pages 5–21.

[19] P.R. Spalart, F.T. Johnson, and S.R. Allmaras. Modifications and clarifications for the implementation of the Spalart-Allmaras turbulence model. *7th International Conference on Computational Fluid Dynamics, Big Island, Hawaii*, 2012.

[20] M. Ferlauto and R. Marsilio. A computational approach to the simulation of controlled flows by synthetic jets actuators. *Advances in Aircraft and Spacecraft Science*, (2014), **2(1)**:77–94.

[21] V. Vatsa and E. Turkel. Simulation of synthetic jets using unsteady Reynolds-averaged Navier-Stokes equations. *AIAA Journal*, (2006), **44**:217–224.

[22] C. Tian and Y. Lu. Turbulence models of separated flow in shock wave thrust vector nozzle. *Engineering Applications of Computational Fluid Mechanics*, (2013), **7(2)**:182–192.

[23] A. Harten, E. Engquist, and S. Osher. Uniformly high order accurate essentially non-oscillatory schemes. *Journal of Computational Physics*, (1987), **71**:231–303.

[24] M. Ferlauto. A pseudo-compressibility method for solving inverse problems based on the 3D incompressible euler equations. *Inverse Problems in Science and Engineering*, (2015), **23(5)**:798–817.

[25] M. Ferlauto and R. Marsilio. Computational investigation of injection effects on shock vector control performance. *54th AIAA Joint Propulsion Conference, Cincinnati, Ohio*, 2018.

[26] R.A. Lawrence. Simmetrical and unsymmetrical flow separation in supersonic nozzles. *NASA Contract Report CR-92587*, 1967.

[27] Lawrence R.A. and E Weynand. Factors affecting flow separation in contoured supersonic nozzles. *AIAA Journal*, (1968), **6(6)**:1159–1160.

[28] J.G Ziegler and N.B. Nichols. Optimum settings for automatic controllers. *Transactions of the ASME*, (1942), **64**:759–768.